applied optics

Optical switching and bistability in a degenerated two-level atomic medium under an external magnetic field

Hoang Minh Dong,[1] Luong Thi Yen Nga,[2] and Nguyen Huy Bang[2,*]

[1]Institute of Research and Development, Duy Tan University, Da Nang 550000, Vietnam
[2]Vinh University, 182 Le Duan Street, Vinh City, Vietnam
*Corresponding author: bangnh@vinhuni.edu.vn

Received 14 February 2019; revised 30 April 2019; accepted 30 April 2019; posted 1 May 2019 (Doc. ID 360181); published 22 May 2019

We propose a simple system for both optical switching and bistability based on degenerated two-level atoms placed in a ring cavity and an external magnetic field. The magnetic field splits a lower level into two separated levels, both of which are connected to an upper level by coupling and probe laser fields. Under an electromagnetically induced transparency regime, the system exhibits optical bistability and switching properties in which its thresholds and switching rate can be controlled by modulating intensity of the magnetic field or the coupling light field. Furthermore, the system can be controlled to work in varying frequency regimes by using a sole laser for both coupling and probe fields. Such a proposed scheme may be useful for realization of optical switches and storage devices.

https://doi.org/10.1364/AO.58.004192

1. INTRODUCTION

The optical switch is an essential element in optical communication, information networks, and quantum computing [1]. Over the last few decades, all-optical switches based on optical bistability (OB) in two-level atomic systems have been studied [2]. However, much interest has been focused on multilevel atom systems with a huge number of works relating to quantum coherent phenomena. Among the novel phenomena, the so-called electromagnetically induced transparency (EIT) [3,4] has made significant progress. Because it significantly reduces resonant absorption and sharpens dispersion, the EIT significantly enhances the interaction time between light and matter [5–8], which enhances nonlinear optical processes [9–18] or nonlinear optics at low-light level.

From a practical point of view, all-optical switching at low-light intensities based on quantum coherence has favorable advantages compared with conventional electro-optical switching, such as high response speed and low switching thresholds. In this context, Schmidt and Ram [19] proposed a way for implementation of an all-optical switching modulator and converter in a three-level system based on EIT. Subsequently, Ham and co-workers suggested techniques for the generation of all-optical switching based on the creation of dark states in a three-level system [20] and four-level system [21] in ion-doped crystals. Moreover, Li *et al.* [22] also demonstrated that OB can be controlled efficiently in a four-subband quantum well system via tuning the coupling strength of the tunneling and Fano-type interference. On the other hand, using a two-photon absorption scheme in an alkali-metal vapor cell, Yavuz [23] suggested a technique where a strong laser beam switches off another laser beam in femtosecond time scales. Furthermore, Antón *et al.* [24] proposed a method for all-optical switching with a technique based on controlled double-dark resonances. Li *et al.* [25] investigated light propagation and operation of magneto-optics in a four-level inverted-Y atomic medium. Recently, low-light-level optical switching and bistability schemes have also been extensively investigated [26–29].

Despite the extensive proposals on this topic for multi-level energy atoms, in which all interacting fields must be controlled synchronously, there is a need for a simpler excitation scheme, e.g., two-level, for comfortable realization. Furthermore, studies often neglect degeneration of Zeeman levels, which should be considered when atoms are immersed in external magnetic fields or polarized optical fields. Growing in this interest, in this work, we propose a simple model for both optical switching and bistability based on a degenerated two-level system under assistance of a static magnetic field and EIT. We address how the absorption characteristics of the medium under magnetic field interact, which can result in optical switches and bistability. In our model, the OB threshold can be controlled by both the magnetic field and coupling field intensity as well as the detuning of the applied fields. Then, by simultaneously solving the coupled Maxwell–Bloch equations, it is found that in the absence of a magnetic field, the system exhibits transparency for the probe field. In this condition, the weak probe

beam of light can propagate without attenuation in the medium. In the presence of the magnetic field, the medium becomes completely absorptive due to interacting dark resonances. The suggested scheme may be useful in applications of magneto-optic switches and magneto-optic storage devices in processing telecommunication signals.

2. MODEL AND BASIC EQUATIONS

We consider a degenerated two-level lambda atomic system under interaction of an external magnetic field, as shown in Fig. 1. A weak probe laser field E_p with the left-circularly polarized component σ^- (with carrier frequency ω_p and a one-half Rabi-frequency $\Omega_p = \mu_{21}E_p/2\hbar$) drives the transition $|1\rangle - |2\rangle$. At the same time, a strong coupling laser field E_c with the right-circularly polarized component σ^+ (with carrier frequency ω_c a one-half Rabi-frequency $\Omega_c = \mu_{23}E_c/2\hbar$) applies the transition $|3\rangle - |2\rangle$. In this configuration (Fig. 1), the probe field travels in the same direction as the magnetic field B, which is used to lift up level $|3\rangle(m_F = +1)$ and to pull down level $|1\rangle(m_F = -1)$ via the Zeeman effect. The Zeeman shift of levels $|1\rangle$ and $|3\rangle$ is given by $\hbar\Delta_B = \mu_B m_F g_F B$, where μ_B is the Bohr magneton, g_F is the Landé factor, and $m_F = \pm 1$ is the magnetic quantum number. All the atoms are assumed initially in states $|1\rangle$ and $|3\rangle$ with the same populations, i.e., $\rho_{11} = \rho_{33} = 1/2$ [25,30]. The decay rates from states $|2\rangle$ and $|1\rangle$, and $|2\rangle$ to $|3\rangle$ are given by γ_{21} and γ_{23}, respectively. The relaxation rates between ground states $|1\rangle$ and $|3\rangle$ by collisions are negligible.

Using the rotating-wave and the electric dipole approximations, the Hamiltonian of the system in the interaction picture can be written as (with the assumption of $\hbar = 1$)

$$H_{\text{int}} = \begin{bmatrix} 0 & -\Omega_p^* & 0 \\ -\Omega_p & \Delta_p + \Delta_B & -\Omega_c^* \\ 0 & -\Omega_c & (\Delta_p + \Delta_B) - (\Delta_c - \Delta_B) \end{bmatrix}, \quad (1)$$

where $\Delta_p = \omega_{21} - \omega_p$ and $\Delta_c = \omega_{23} - \omega_c$ are detunings of the probe field and coupling field from the atomic transition frequencies, respectively; Δ_B is the Zeeman shift of levels $|1\rangle$ and $|3\rangle$ in the presence of the magnetic field [see Fig. 1(b)], and Δ_B is taken to zero for zero magnetic field. The dynamical evolution of the system can be described by the Liouville equation:

$$\frac{\partial \rho}{\partial t} = -i[H_{\text{int}}, \rho] + \Lambda\rho, \quad (2)$$

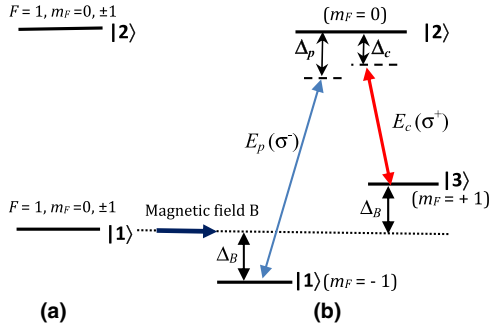

Fig. 1. Degenerated two-level (a) and forming the three-level lambda (b) under a static magnetic field.

and the relevant density matrix equations obtained for this system are given as follows:

$$\frac{\partial \rho_{11}}{\partial t} = \gamma_{21}\rho_{22} + i\Omega_p^*\rho_{21} - i\Omega_p\rho_{12}, \quad (3a)$$

$$\frac{\partial \rho_{22}}{\partial t} = -(\gamma_{21} + \gamma_{23})\rho_{22} + i\Omega_p\rho_{12} - i\Omega_p^*\rho_{21} + i\Omega_c\rho_{32} - i\Omega_c^*\rho_{23}, \quad (3b)$$

$$\frac{\partial \rho_{33}}{\partial t} = \gamma_{23}\rho_{22} + i\Omega_c^*\rho_{23} - i\Omega_c\rho_{32}, \quad (3c)$$

$$\frac{\partial \rho_{21}}{\partial t} = -\left(i(\Delta_p + \Delta_B) + \frac{\gamma_{21} + \gamma_{23}}{2}\right)\rho_{21} - i\Omega_p(\rho_{22} - \rho_{11}) + i\Omega_c\rho_{31}, \quad (3d)$$

$$\frac{\partial \rho_{31}}{\partial t} = -i(\Delta_p - \Delta_c + 2\Delta_B)\rho_{31} - i\Omega_p\rho_{32} + i\Omega_c^*\rho_{21}, \quad (3e)$$

$$\frac{\partial \rho_{23}}{\partial t} = -\left(i(\Delta_c - \Delta_B) + \frac{\gamma_{21} + \gamma_{23}}{2}\right)\rho_{23} - i\Omega_c(\rho_{22} - \rho_{33}) + i\Omega_p\rho_{13}, \quad (3f)$$

where the matrix elements obey conjugated and normalized conditions, namely, $\rho_{ij} = \rho_{ij}^*$ $(i \neq j)$ and $\rho_{11} + \rho_{22} + \rho_{33} = 1$, respectively.

3. RESULTS AND DISCUSSION

In order to illustrate applications of the model, we use the cold atomic medium of ^{87}Rb [31]. States $|1\rangle$, $|2\rangle$, and $|3\rangle$ are chosen as $5S_{1/2}(F = 1, m_F = 1)$, $5P_{1/2}(F = 1, m_F = 0)$, and $5S_{1/2}(F = 1, m_F = -1)$, respectively. The decaying rates are $\gamma_{21} = \gamma_{23} = 2\pi \times 5.3$ MHz and laser wavelengths $\lambda_p = \lambda_c = 795$ nm. The Landé factor $g_F = -1/2$, and the Bohr magneton $\mu_B = 9.27401 \times 10^{-24}$ JT^{-1} [31]. We also scale the Zeeman shift Δ_B by γ_{21}, then the magnetic field strength B should be in units of the combined constant $\gamma_c = \hbar\mu_B^{-1}g_F^{-1}\gamma_{21}$.

A. Probe Absorption Behaviors under Magnetic Field

First, we consider the influence of the magnetic field on the absorption behaviors of the probe field in the presence of the coupling field by numerically solving the above density matrix Eqs. (3a)–(3f) in the steady state. As shown in Fig. 2, the absorption behaviors of the probe fields depend on the magnetic field. Indeed, when the magnetic field is absent, i.e., $B = 0$, the probe absorption can be completely suppressed at the resonant center; thus, the medium becomes transparent (dashed line in Fig. 2). This is due to destructive interference between the transitional probability channels induced by the coupling and probe fields (the EIT effect). However, the EIT window is shifted to the blue [Fig. 2(a)] or the red [Fig. 2(b)] by an amount of $2\Delta_B$ when the magnetic field is turned on with $B = 2\gamma_c$ or $B = -2\gamma_c$, respectively (while keeping the coupling field's frequency unchanged). This shift can be explained by the two-photon resonance condition for EIT under Zeeman splitting [5], namely, $\Delta_p - \Delta_c + 2\Delta_B = 0$. Consequently,

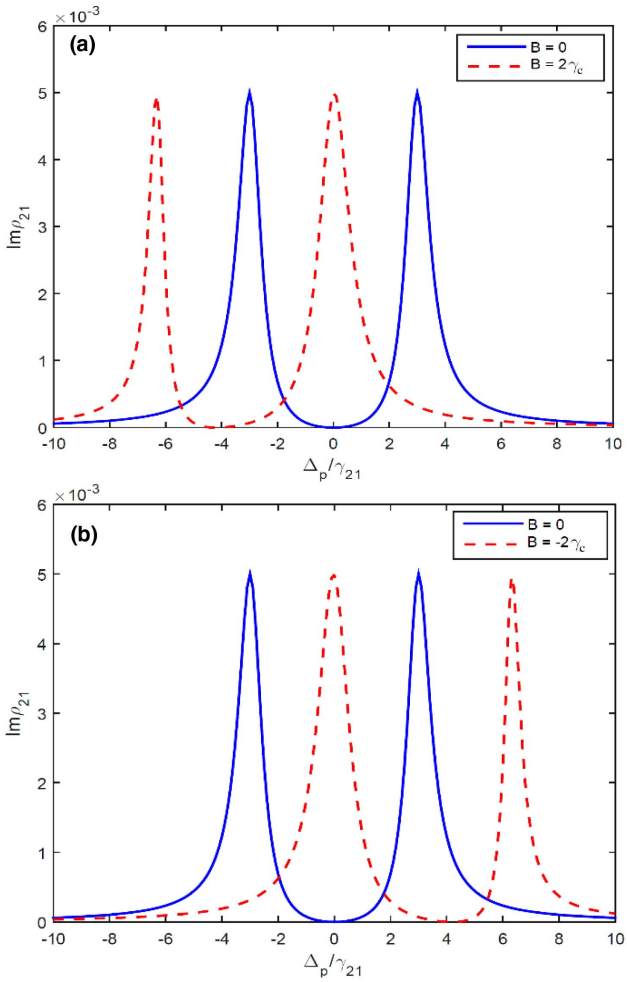

Fig. 2. Probe absorption coefficients versus the probe detuning Δ_p for the absence $B = 0$ (red dashed line) and presence (blue solid line) of the magnetic field: (a) $B = 2\gamma_c$ and (b) $B = -2\gamma_c$. Other system parameters are chosen as $\Omega_p = 0.01\gamma_{21}$, $\Omega_c = 3\gamma_{21}$, and $\gamma_{23} = \gamma_{21}$, respectively.

by choosing proper magnetic strengths and its direction, one can switch the medium from the strong absorptive to transparent mode, and vice versa. Furthermore, the EIT window can be shifted variously to red or blue side by tuning the magnetic field without variation of the coupling light. This controllable behavior is very important for controlling optical bistability and optical switching in the degenerated two-level system.

B. Control of Optical Bistability

Now, we put this atomic sample inside a unidirectional ring cavity comprising four mirrors, as shown in Fig. 3. For simplicity, we assume that mirrors 3 and 4 have 100% reflectivity, and the reflection intensity and transmission coefficient of mirrors 1 and 2 are R and T (with $R + T = 1$), respectively. For a perfectly tuned ring cavity, in the steady-state limit, the boundary conditions impose the following conditions between the incident field E_p^I and the transmitted field E_p^T [27]:

$$E_p(L) = E_p(T)/\sqrt{T}, \tag{4a}$$

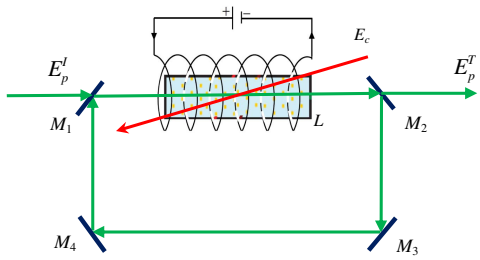

Fig. 3. Unidirectional ring cavity containing an atomic sample of length L; E_p^I and E_p^T are the incident and the transmitted fields, respectively.

$$E_p(0) = \sqrt{T}E_p^I + RE_p(L), \tag{4b}$$

where L is the atomic sample length, and the second term on the right-hand side of Eq. (4b) describes a feedback mechanism that gives rise to bistability. In the mean-field limit, using the boundary conditions, Eq. (4), and normalizing the fields by letting $y = \mu_{21}E_p^I/\hbar\sqrt{T}$ and $x = \mu_{21}E_p^T/\hbar\sqrt{T}$, we can get the input–output relationship

$$y = x - iC\rho_{21}, \tag{5}$$

where $C = \omega_p L|\mu_{21}|^2 N/2\hbar\varepsilon_0 cT$ is the cooperation parameter. It is known that the second term on the right-hand side of Eq. (5) is necessary to the appearance of OB.

In this section, we will analyze the influence of the magnetic field B on the shape of the OB curve. It is easy to see in Fig. 4(a) that the threshold of OB first increases dramatically, and the threshold width becomes wider as the intensity of the external magnetic field increases and then decreases gradually. In order to gain deeper insight into this change, we plot the absorption coefficients of the probe field $\mathrm{Im}(\rho_{21})$ versus the magnetic field strength B, as shown in Fig. 4(b). When the magnetic field B is absent (i.e., $B = 0$), levels $|1\rangle$ and $|3\rangle$ are degenerated. The absorption of the degenerate two-level medium under EIT is suppressed maximally, and there is no OB [Fig. 4(a)] because of the absorptive bistability [27]. With the increase in strength of the magnetic field, the level splitting between $|1\rangle$ and $|3\rangle$ is enhanced, and the quantum interference between the two transition pathways $|1\rangle \to |2\rangle$ and $|3\rangle \to |2\rangle$ is reduced, which increases the absorption of the probe field. When magnetic field B increases to the value $B = 2\gamma_c$, the absorption of the probe field reaches a maximal value, and the bistable threshold reaches to the maximum [the star line in Fig. 4(b)]. When B further increases, the magnitude of the probe absorption is decreased dramatically and finally trends to a small steady-state value, the bistable threshold decreases slowly. As such, the threshold value and the hysteresis cycle width of the bistable curve can be controlled by properly adjusting the magnetic field.

Figure 5 illustrates the dependence of the OB on the intensity of the coupling field Ω_c Fig. 5(a) and on the atomic cooperation parameter C Fig. 5(b), respectively. It is easy to see in Fig. 5(a) that the bistable threshold is dramatically increased as the intensity of the coupling field increases, and then decreases gradually. When the coupling field Ω_c increases from $1\gamma_{21}$ to a certain value (Ω_c is around $3\gamma_{21}$), the absorption of the probe field reaches a saturation value, and the bistable

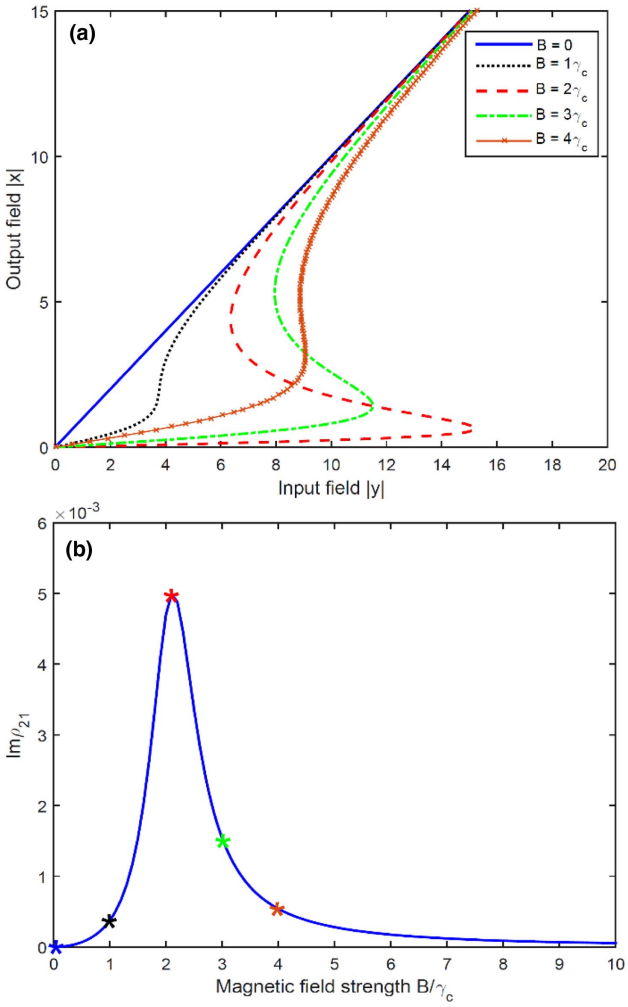

Fig. 4. Output field $|x|$ versus input field $|y|$ for different values of the magnetic field (a) and variation of the absorption versus magnetic field strength (b). The parameters are: $\Omega_p = 0.01\gamma_{21}$, $\Omega_c = 3\gamma_{21}$, $\Delta_c = \Delta_p = 0$, and $\gamma_{23} = \gamma_{21}$, respectively.

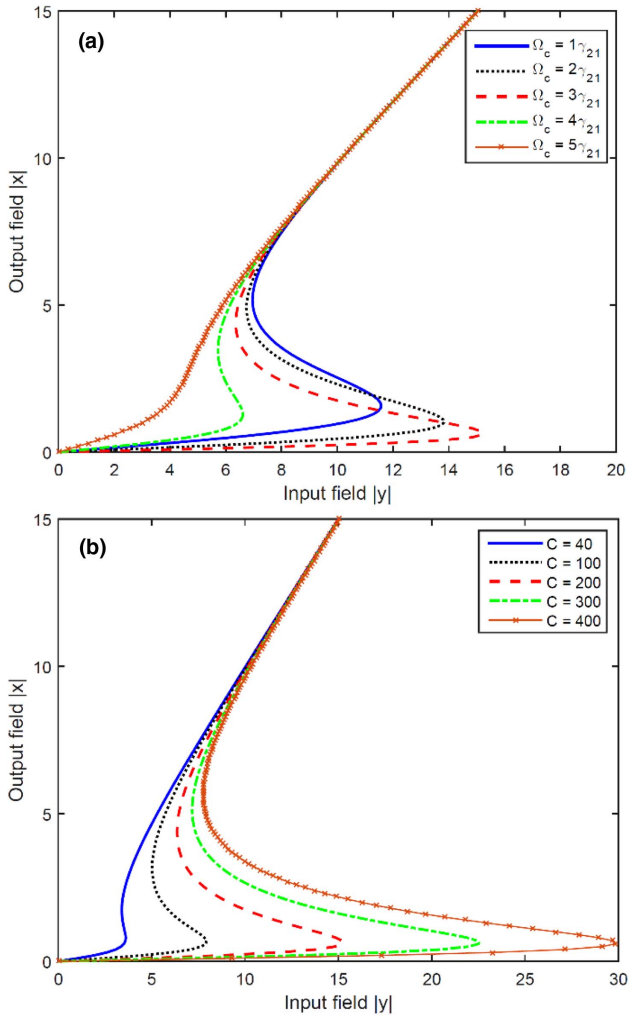

Fig. 5. Output field $|x|$ versus input field $|y|$ for different values of the coupling field Ω_c [panel (a), with $C = 200$] and for different values of C [panel (b), with $\Omega_c = 3\gamma_{21}$]. Other parameters are: $\Omega_p = 0.01\gamma_{21}$, $\Delta_c = \Delta_p = 0$, $B = 2\gamma_c$, and $\gamma_{23} = \gamma_{21}$, respectively.

threshold reaches the maximum (red curve). However, with Ω_c further increasing, the bistable threshold decreases rapidly, which can be easily explained in that an increasingly coherent control field reduces the absorption for the probe field and enhances nonlinearity of the medium, thus leading to a change in OB behavior. Consequently, one can control the OB threshold by adjusting the intensity of the coherent control field Ω_c. On the other hand, Fig. 5(b) shows the dependence of OB on the cooperation parameter C. As we can see, the cooperation parameter C is directly proportional to the atomic number density N. Therefore, an increase of C leads to an enhancement of the absorption of the sample, which gives rise to dependence of the OB threshold on the cooperation parameter C [27].

In Fig. 6, we show the influence of the frequency detuning of the probe laser and control laser fields on the behavior of OB, while keeping all other parameters fixed. It is clearly shown that with increasing $\Delta_{p,c}$ from 0 to $4\gamma_{21}$, the threshold of OB decreases progressively. Furthermore, the OB disappears with increasing Δ_c to $4\gamma_{21}$. The reason for the above results can be qualitatively interpreted as follows. A gradual increase in frequency detuning $\Delta_{p,c}$ from 0 to $4\gamma_{21}$ leads to a progressive change of the absorption for the probe laser field because of shifting the EIT window to ensure two-photon resonance [similar to the case explained in Fig. 2(a)].

C. Propagation Dynamics and Optical Switching

To be of practical interest and to demonstrate the analysis given in the previous section, in the following, the propagation of a weak probe pulse through the atomic medium is addressed. Under the slowly varying envelope and rotating-wave approximations, evolution of the probe field is represented by the following wave equation [18]:

$$\frac{\partial \Omega_p(z,t)}{\partial z} + \frac{1}{c}\frac{\partial \Omega_p(z,t)}{\partial t} = i\alpha\gamma_{21}\rho_{21}(z,t), \tag{6}$$

where $\alpha = \frac{\omega_p N|d_{21}|^2}{4\varepsilon_0 c\hbar\gamma_{21}}$ is the propagation constant. For convenience, we represent Rabi frequency of the probe field by $\Omega_p(z,t) = \Omega_{p0} f(z,t)$, where Ω_{p0} is a real constant indicating the maximal value of the Rabi frequency at the entrance

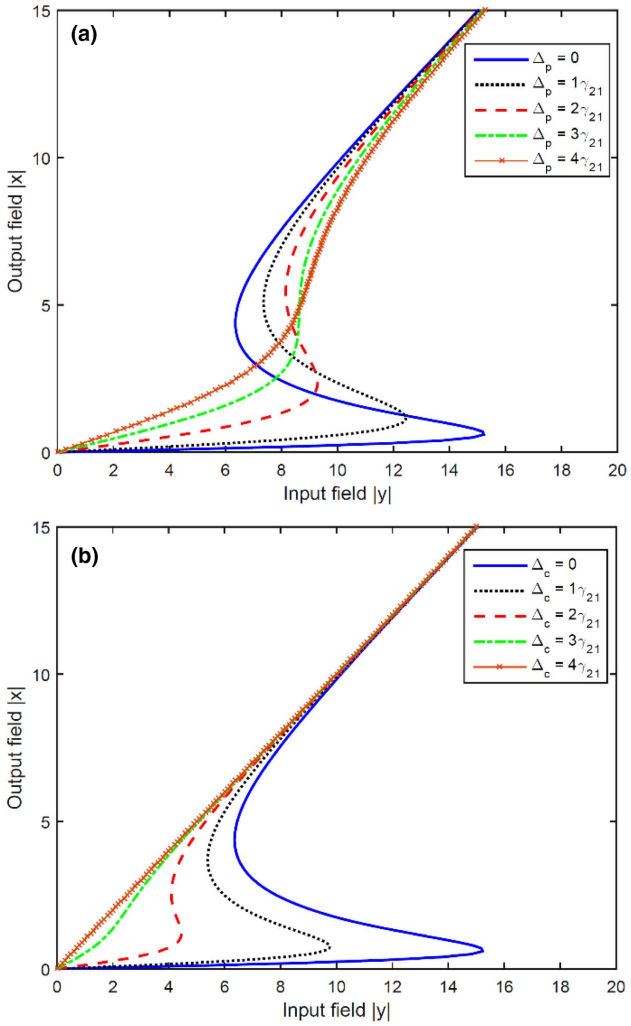

Fig. 6. Output field $|x|$ versus input field $|y|$ for different values of the probe detuning Δp [panel (a), with $\Delta c = 0$], and the control detuning Δ_c [panel (b), with $\Delta_p = 0$]. The parameters are: $\Omega_p = 0.01\gamma_{21}$, $\Omega_c = 3\gamma_{21}$, and $\gamma_{23} = \gamma_{21}$, respectively.

(i.e., at $z = 0$), and $f(z,t)$ is a dimensionless spatiotemporal pulse-shaped function. In a moving frame with $\xi = z$ and $\tau = t - z/c$, the optical Bloch matrix Eqs. (3a)–(3f) for the density elements $\rho_{ij}(\xi,\tau)$ and the Maxwell's wave Eq. (6) for the probe field $f(\xi,\tau)$ can be rewritten as

$$\frac{\partial\rho_{11}}{\partial\tau} = \gamma_{21}\rho_{22} + i\Omega_{p0}f^*(\xi,\tau)\rho_{21} - i\Omega_{p0}f(\xi,\tau)\rho_{12}, \tag{7a}$$

$$\frac{\partial\rho_{22}}{\partial\tau} = -(\gamma_{21}+\gamma_{23})\rho_{22} + i\Omega_{p0}f(\xi,\tau)\rho_{12} - i\Omega_{p0}f^*(\xi,\tau)\rho_{21} + i\Omega_c\rho_{32} - i\Omega_c^*\rho_{23}, \tag{7b}$$

$$\frac{\partial\rho_{33}}{\partial\tau} = \gamma_{23}\rho_{22} + i\Omega_c^*\rho_{23} - i\Omega_c\rho_{32}, \tag{7c}$$

$$\frac{\partial\rho_{21}}{\partial\tau} = -\left(i(\Delta_p+\Delta_B) + \frac{\gamma_{21}+\gamma_{23}}{2}\right)\rho_{21} + i\Omega_c\rho_{31} - i\Omega_{p0}f(\xi,\tau)(\rho_{22}-\rho_{11}), \tag{7d}$$

$$\frac{\partial\rho_{31}}{\partial\tau} = -i(\Delta_p - \Delta_c + 2\Delta_B)\rho_{31} - i\Omega_{p0}f(\xi,\tau)\rho_{32} + i\Omega_c^*\rho_{21}, \tag{7e}$$

$$\frac{\partial\rho_{23}}{\partial\tau} = -\left(i(\Delta_c-\Delta_B) + \frac{\gamma_{21}+\gamma_{23}}{2}\right)\rho_{23} - i\Omega_c(\rho_{22}-\rho_{33}) + i\Omega_{p0}f(\xi,\tau)\rho_{13}, \tag{7f}$$

$$\frac{\partial f(\xi,\tau)}{\partial(\alpha\xi)} = i\frac{\gamma_{21}}{\Omega_{p0}}\rho_{21}(\xi,\tau). \tag{7g}$$

In the following, we solve numerically the set of Eq. (7) on a space–time grid by using a combination of the four-order Runge–Kutta and finite difference methods, which developed a computer code for this problem is expanded from the of our previous work [18]. The boundary condition for the probe pulse is a Gaussian-type shape:

$$f(\xi=0,\tau) = \exp[-(\ln 2)(\tau-30)^2/\tau_0^2], \tag{8}$$

where $\tau_0 = 6/\gamma_{21}$ is the temporal width of the pulse at the entrance of the medium.

In Fig. 7, we plot the temporal evolution of the magnitude squared of the normalized probe pulse envelope $|f(\xi,\tau)|^2$ at the exit of the medium $\xi = 30/\alpha$ for the modulation cases of magnetic field and control field intensity. In Fig. 7(a) can be seen that the switching off and on of the magnetic field significantly affects the amount of probe pulse absorption during propagation in the medium. With a gradual increase in the intensities of the magnetic field, the absorption of the probe pulse increases considerably. Specifically, for the case in which the magnetic field is turned off (i.e., $B = 0$), the absorption of the probe pulse can be suppressed, and the atomic medium is almost transparent to the probe pulse after a characteristic propagation length (blue solid line). In contrast, for the case in which $B \neq 0$, namely, when the magnetic field is turned on, the probe pulse is absorbed obviously at the exit of the medium. When the intensity of the magnetic field increases to around value $B = 2\gamma_c$ (red dashed line), the probe pulse can be completely absorbed by the medium in a short propagation distance. However, when the intensity of the magnetic field continuously increases larger $B > 2\gamma_{21}$, the probe absorption is decreased (see green and magenta lines). As a result, by suitably varying the magnetic field, we can realize magneto-optical modulation for such a probe pulsed signal. In Fig. 7(b), for the cases in which $\Omega_c = 1\gamma_{21}$ and $2\gamma_{21}$, the probe pulse is gradually depleted and completely absorbed with $\Omega_c = 3\gamma_{21}$. When the coupling field intensity continues to increase [e.g., $\Omega_c = 4\gamma_{21}$, and $5\gamma_{21}$], the absorption of the probe pulse decreases considerably.

In Fig. 8, we show the temporal evolution of the magnitude squared of the normalized probe pulse envelope $|f(\xi,\tau)|^2$ at the exit of the medium $\xi = 30/\alpha$ for the varying cases of the probe field and control field detuning. In the figure, one can see that the absorption of the probe pulse decreases considerably with a gradual increase of the detuning of the applied field. Furthermore, the probe detuning is more than significantly influenced compared to the detuning of the control field.

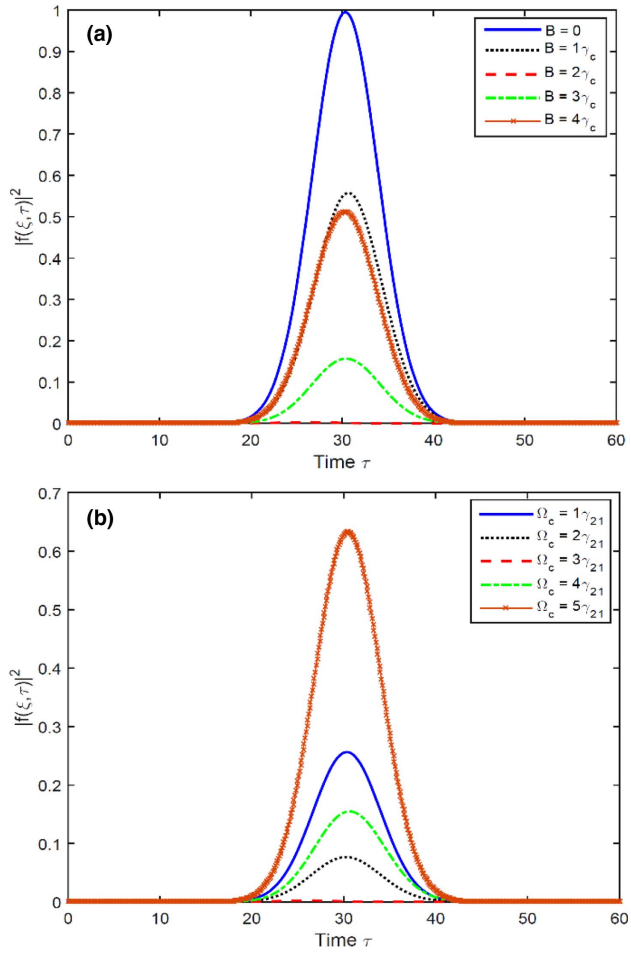

Fig. 7. Magnitude squared of probe pulse envelopes at the exit of the medium $\xi = 30/\alpha$ for different values of the magnetic field B [panel (a), $\Omega_c = 3\gamma_{21}$] and for different values of the control field Ω_c [panel (b), $B = 2\gamma_c$]. Other parameters are $\Omega_{p0} = 0.01\gamma_{21}$, $\Delta_p = \Delta_c = 0$, and $\gamma_{23} = \gamma_{21}$; time τ and propagation distance ξ are calculated in units of γ_{21}^{-1} and α^{-1}, respectively.

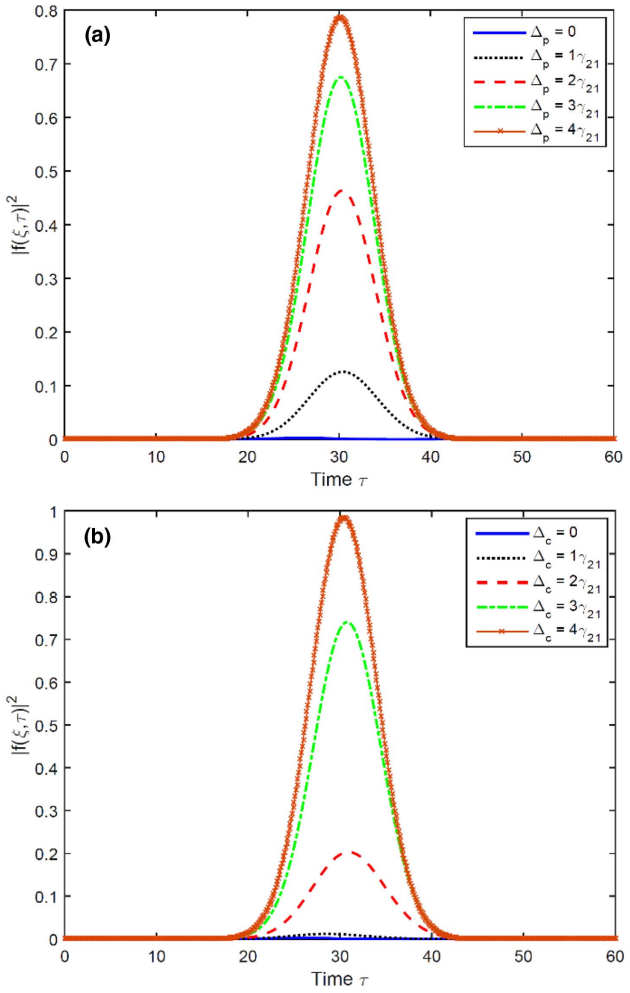

Fig. 8. Magnitude squared of probe pulse envelopes at the exit of the medium $\xi = 30/\alpha$ for different values of the probe detuning Δ_p [panel (a), $\Delta_c = 0$] and for different values of the control detuning Δ_c [panel (b), $\Delta_p = 0$]. Other parameters are $\Omega_{p0} = 0.01\gamma_{21}$, $\Omega_c = 3\gamma_{21}$, $B = 2\gamma_c$, and $\gamma_{23} = \gamma_{21}$, respectively.

Figure 9 shows the spatiotemporal evolution of the magnitude squared of the normalized probe pulse envelope $|f(\xi,\tau)|^2$ via modulating the intensity of the external magnetic field as the probe laser pulse propagates through atomic medium under the conditions in which the $\Omega_c = 3\gamma_{21}$, $\Delta_c = \Delta_p = 0$. As can be seen in Fig. 9, the switching off and on of the magnetic field affects strongly the probe pulse absorption during propagation in the medium. Specifically, for the case in which no external magnetic field exists [i.e., $B = 0$], the atomic medium is transparent to the probe pulse, which propagates over sufficiently long distances. Furthermore, the pulse shape remains Gaussian on propagation [see Fig. 9(a)]. In contrast, when the external magnetic field is applied $B = 2\gamma_c$, the probe pulse can be completely absorbed by the medium in a very short propagation distance. These results are consistent with the absorption spectral profile of the probe field given in Figs. 2, 4(b), and 7. Therefore, the medium can be switched between a strong absorptive and transparent mode by switching the magnetic field on and off, respectively.

Finally, we consider a possible way to realize optical switching for the probe field by tuning the magnetic field, as shown in Fig. 10. Here, the probe field (solid lines) is assumed to be a continuous wave, whereas the switching magnetic field (dashed lines) is a nearly square pulse with smooth rising and falling edges: $B(\tau) = B_0\{1 - 0.5[\tan \hbar 0.4(\tau - 20) + \tan \hbar 0.4(\tau - 45) - \tan \hbar 0.4(\tau - 70) + \tan \hbar 0.4(\tau - 95)]\}$. The magnetic field is normalized by its peak value B_0, with an approximate period of $50/\gamma_{21}$. As shown in Fig. 10, the probe transmission is switched to either ON or OFF mode when the magnetic field is OFF or ON, respectively. This behavior can be explained by noting that the presence or absence of the magnetic field can switch, respectively, the medium to a strong absorptive or transparent mode due to the Zeeman shift of levels $|1\rangle$ and $|3\rangle$, which shift the EIT window followed by two-photon resonance.

4. POSSIBLE EXPERIMENTAL REALIZATION

In this section, we discuss a possible experimental realization for the case of ^{87}Rb atoms on the $5S_{1/2} \leftrightarrow 5P_{1/2}$ transitions.

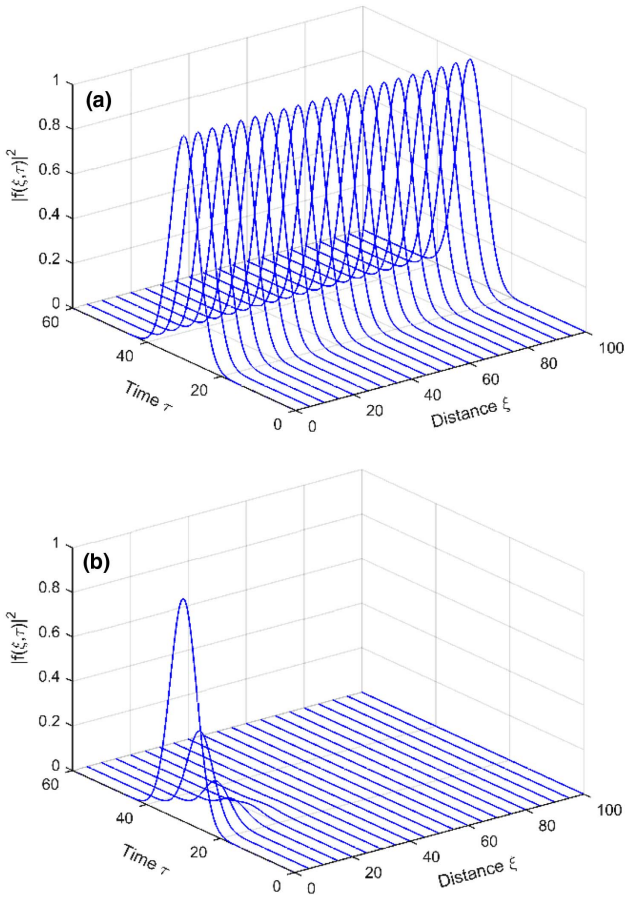

Fig. 9. Space–time evolution of normalized probe field intensity for the absence and presence of the magnetic field: $B = 0$ for (a), and $B = 2\gamma_c$ for (b). Other parameters are $\Omega_{0p} = 0.01\gamma_{21}$, $\Omega_c = 3\gamma_{21}$, $\Delta_p = \Delta_c = 0$, and $\gamma_{23} = \gamma_{21}$, respectively.

The excitation scheme and experiment can be arranged as in Figs. 1 and 3, respectively. Here, states $|1\rangle$, $|2\rangle$, and $|3\rangle$ are given as $5S_{1/2}(F = 1, m_F = -1)$, $5S_{1/2}(F = 1, m_F = 1)$, and $5P_{1/2}(F = 1, m_F = 0)$, respectively. For the case of the optical switching, the feedback arm of the ring cavity (in Fig. 3) is removed. Both the probe and coupling fields can be used by combination of a single-mode external cavity diode laser (795 nm) and an acousto-optic modulator (AOM). The magnetic field can be generated by using a solenoid tube connected with a variation DC current source via an interchangeable anode-cathode switch. Due to the Zeeman splitting in opposite directions for levels $5S_{1/2}(F = 1, m_F = -1))$ and $5S_{1/2}(F = 1, m_F = +1)$, the first-order blue shift and red shift output beams from the AOM can be used to deliver the coupling and probe lights, respectively.

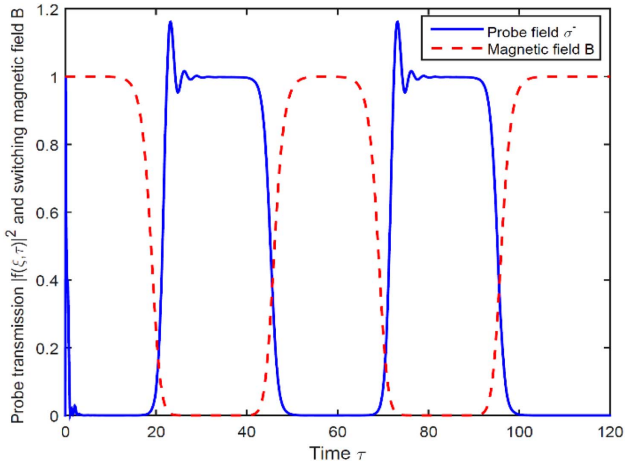

Fig. 10. Time evolution of a cw probe field (solid line) at $\xi = 30/\alpha$ when the magnetic field (dashed lines) switches at period $50/\gamma_{31}$. Other parameters are $f(\xi = 0, \tau) = 1$, $\Omega_{p0} = 0.01\gamma_{21}$, $\Omega_c = 3\gamma_{21}$, $B_0 = 2\gamma_c$, and $\Delta_p = \Delta_c = 0$, respectively.

In order to ensure selection rules for the excitation configuration, the coupling and probe beams are directed to quarter-wave plates to produce σ^- (probe beam) and σ^+ (coupling) polarized beams where both of which propagate in opposite directions (see Fig. 3).

5. CONCLUSION

We have proposed a simple system for both optical switching and bistability based on degenerated two-level atoms placed in a ring cavity and an external magnetic field. The magnetic field splits a lower level into two separated levels, both of which are connected to an upper level by a coupling and probe laser fields. It is shown that under the EIT regime, the system exhibits optical bistability and switching properties in which its thresholds and switching rate can be controlled by modulating intensity of the magnetic field or the coupling light field. Furthermore, due to symmetry of Zeeman splitting and the AOM effect, the system can be controlled to work in varying frequency regimes by using a sole laser for both coupling and probe fields. Such a proposed scheme may be useful for realization of optical switches and storage devices.

Funding. Ministry of Science and Technology (MOST) (ĐTĐLCN.17/17).

REFERENCES

1. H. Ishikawa, *Ultrafast All-Optical Signal Processing Devices* (Wiley, 2008).
2. H. M. Gibbs, S. L. McCall, and T. N. C. Venkatesan, "Differential gain and bistability using a sodium-filled Fabry-Perot interferometer," Phys. Rev. Lett. **36**, 1135–1138 (1976).
3. A. Imamoğlu and S. E. Harris, "Lasers without inversion: interference of dressed lifetime broadened states," Opt. Lett. **14**, 1344 (1989).
4. K.-J. Boller, A. Imamoğlu, and S. E. Harris, "Observation of electromagnetically induced transparency," Phys. Rev. Lett. **66**, 2593–2596 (1991).
5. M. Fleischhauer, A. Imamoglu, and J. P. Marangos, "Electromagnetically induced transparency: optics in coherent media," Rev. Mod. Phys. **77**, 633–673 (2005).
6. L. V. Doai, P. V. Trong, D. X. Khoa, and N. H. Bang, "Electromagnetically induced transparency in five-level cascade scheme of ^{85}Rb atoms: an analytical approach," Optik **125**, 3666–3669 (2014).
7. D. X. Khoa, P. V. Trong, L. V. Doai, and N. H. Bang, "Electromagnetically induced transparency in a five-level cascade system under Doppler broadening: an analytical approach," Phys. Scr. **91**, 035401 (2016).
8. D. X. Khoa, L. C. Trung, P. V. Thuan, L. V. Doai, and N. H. Bang, "Measurement of dispersive profile of a multi-window EIT spectrum

in a Doppler-broadened atomic medium," J. Opt. Soc. Am. B. **34**, 1255 (2017).
9. N. T. Anh, L. V. Doai, and N. H. Bang, "Manipulating multi-frequency light in a five-level cascade-type atomic medium associated with giant self-Kerr nonlinearity," J. Opt. Soc. Am. B **35**, 1233 (2018).
10. D. X. Khoa, L. V. Doai, D. H. Son, and N. H. Bang, "Enhancement of self-Kerr nonlinearity via electromagnetically induced transparency in a five-level cascade system: an analytical approach," J. Opt. Soc. Am. B. **31**, 1330 (2014).
11. L. V. Doai, D. X. Khoa, and N. H. Bang, "EIT enhanced self-Kerr nonlinearity in the three-level lambda system under Doppler broadening," Phys. Scr. **90**, 045502 (2015).
12. H. R. Hamedi, A. H. Gharamaleki, and M. Sahrai, "Colossal Kerr nonlinearity based on electromagnetically induced transparency in a five-level double-ladder atomic system," Appl. Opt. **55**, 5892 (2016).
13. G. Huang, K. Jiang, M. G. Payne, and L. Deng, "Formation and propagation of coupled ultraslow optical soliton pairs in a cold three-state double-Λ-system," Phys. Rev. E **73**, 056606 (2006).
14. L.-G. Si, X.-Y. Lu, X. Hao, and J.-H. Li, "Dynamical control of soliton formation and propagation in a Y-type atomic system with dual ladder-type electromagnetically induced transparency," J. Phys. B **43**, 065403 (2010).
15. Y. Chen, Z. Bai, and G. Huang, "Ultraslow optical solitons and their storage and retrieval in an ultracold ladder-type atomic system," Phys. Rev. A **89**, 023835 (2014).
16. H. M. Dong, L. V. Doai, V. N. Sau, D. X. Khoa, and N. H. Bang, "Propagation of laser pulse in a three-level cascade atomic medium under conditions of electromagnetically induced transparency," Photonics Lett. Pol. **8**, 73 (2016).
17. D. X. Khoa, H. M. Dong, L. V. Doai, and N. H. Bang, "Propagation of laser pulse in a three-level cascade inhomogeneously broadened medium under electromagnetically induced transparency conditions," Optik **131**, 497–505 (2017).
18. H. M. Dong, L. V. Doai, and N. H. Bang, "Pulse propagation in an atomic medium under spontaneously generated coherence, incoherent pumping, and relative laser phase," Opt. Commun. **426**, 553–557 (2018).
19. H. Schmidt and R. J. Ram, "All-optical wavelength converter and switch based on electromagnetically induced transparency," Appl. Phys. Lett. **76**, 3173–3175 (2000).
20. B. S. Ham, "Nonlinear optics of atoms and electromagnetically induced transparency: dark resonance based optical switching," J. Mod. Opt. **49**, 2477–2484 (2002).
21. S. A. Moiseev and B. S. Ham, "Quantum manipulation of two-color stationary light: quantum wavelength conversion," Phys. Rev. A **73**, 033812 (2006).
22. J.-H. Li, "Controllable optical bistability in a four-subband semiconductor quantum well system," Phys. Rev. B **75**, 155329 (2007).
23. D. D. Yavuz, "All-optical femtosecond switch using two-photon absorption," Phys. Rev. A **74**, 053804 (2006).
24. M. A. Antón, F. Carreño, O. G. Calderón, S. Melle, and I. Gonzalo, "Optical switching by controlling the double-dark resonances in a N-tripod five-level atom," Opt. Commun. **281**, 6040–6048 (2008).
25. J. Li, R. Yu, L. Si, and X. Yang, "Propagation of twin light pulses under magneto-optical switching operations in a four-level inverted-Y atomic medium," J. Phys. B **43**, 065502 (2010).
26. R. Yu, J. Li, C. Ding, and X. Yang, "Dual-channel all-optical switching with tunable frequency in a five-level double-ladder atomic system," Opt. Commun. **284**, 2930–2936 (2011).
27. D. X. Khoa, L. V. Doai, L. N. M. Anh, L. C. Trung, P. V. Thuan, N. T. Dung, and N. H. Bang, "Optical bistability in a five-level cascade EIT medium: an analytical approach," J. Opt. Soc. Am. B **33**, 735 (2016).
28. H. Jafarzadeh, "All-optical switching in an open V-type atomic system," Laser Phys. **27**, 025204 (2017).
29. H. R. Hamedi, "Optical switching, bistability and pulse propagation in five-level quantum schemes," Laser Phys. **27**, 066002 (2017).
30. D. Petrosyan and Y. P. Malakyan, "Magneto-optical rotation and cross-phase modulation via coherently driven four-level atoms in a tripod configuration," Phys. Rev. A **70**, 023822 (2004).
31. D. A. Steck, "Rubidium 87 D line data," http://steck.us/alkalidata.